SF2A 2007
J. Bouvier, A. Chalabaev, C. Charbonnel (eds)

CHARACTERIZING THE MRI-DRIVEN TURBULENT TRANSPORT IN ASTROPHYSICAL DISKS.

G. Lesur[1] and P-Y. Longaretti[1]

Abstract. Since 1990, the magneto-rotational instability (MRI) has been widely recognized as the most promising process to provide a turbulent transport satisfying the observational constraints. Although nearly all disk models make reference to this instability as the source of turbulence, some important aspects of the MRI-driven turbulent state and related effective viscous and resistive transport efficiencies are not well-known. I present recent results on this issue, based on local simulations of the MRI performed with a new MHD spectral code. These results focus on the role of finite (microscopic) resistivity and viscosity on the large-scale turbulent Reynolds and Maxwell stresses, and on the mean large scale electromotive force. This work is expected to give better constraints on turbulent transport, in particular on turbulent resistivity and its anisotropy, which are critically needed for future large scale disk/jets models and simulations.

1 Introduction

The origin of angular transport in accretion disks has always been a central problem in the disk community. The first α model (Shakura & Sunyaev 1973) already assumed a strong level of turbulence, leading to an effective viscosity orders of magnitude higher than molecular viscosity. However, the physical origin of this turbulence in disks is still highly debated. Since unstratified keplerian flows are known to be linearly stable with respect to small perturbations, the existence of an hypothetical nonlinear instability has often been proposed; such an finite amplitude instability may trigger turbulence with finite amplitude perturbations. This question was studied both experimentally (Richard & Zahn 1999) and numerically (Balbus et al 1996; Hawley et al 1999) but recent results showed that the transport due to this instability would be far too low to account for the observational contraints (Lesur & Longaretti 2005).

An MHD instability relevant to accretion disks was found by Balbus & Hawley (1991), the magnetorotational instability (MRI). This instability has been extensively studied since then, mainly with local unstratified (Hawley et al 1995) and stratified (Stone et al 1996) 3D simulations, and global (Hawley 2000) disk simulations. However, the dissipation of turbulent fields in these simulations is not controlled : no physical term is introduced to take care of viscosity and resistivity in a self-consistent way. One may wonder whether the numerical dissipation introduced by these simulations had an impact on the statistical quantities they predic for disk models, such as the effective transport coefficients.

This issue is adressed here, using a 3D spectral Fourier code, with a full control over viscosity, resistivity and numerical dissipation. We first describe the physics and the numerical methods we used to study turbulence in disks. Then, we present new results on the role of magnetic Prandtl number in various magnetic field configuration, which may have strong implications for real accretion disk dynamics. Last, a brief discussion is provided, exhibiting numerical artifact that may influence our results.

2 Methodology

2.1 Physics

All the local MRI simulations performed to date rely on the so called "shearing sheet" configuration (Goldreich & Lynden-Bell 1965 ; Hawley & al 1995), consisting of a 3D periodic box including the mean keplerian shear

[1] Laboratoire d'Astrophysique de Grenoble, UJF CNRS, BP 53 38041 Grenoble CEDEX 9 FRANCE

and rotation. In this approximation, one can easily check that the mean magnetic field direction and strength are time-independent. However, since the mean magnetic field at the local scale is not conserved in real disks, one has to check that this particular behavior of the shearing box doesn't bias the results, in particular in terms of turbulence efficiency. In the following, we will consider essentially the non-zero mean vertical field case ($\langle B_z \rangle = B_o$). Some zero mean field cases will also be discussed for comparison purposes.

For this work, we use a spectral code to solve numerically the MHD equation taking into account a finite viscosity (ν) and resistivity (η). Assuming the cartesian coordinates x, y and z correspond respectively to the ϕ, $-r$, z direction in polar coordinates, the MHD equations can be written in a shearing box as :

$$\partial_t \boldsymbol{u} + \boldsymbol{u} \cdot \boldsymbol{\nabla} \boldsymbol{u} = -\frac{1}{\rho}\boldsymbol{\nabla} P + \frac{1}{\mu_0 \rho}(\boldsymbol{\nabla} \times \boldsymbol{B}) \times \boldsymbol{B} - 2\boldsymbol{\Omega} \times \boldsymbol{u} - 2\Omega S y \boldsymbol{e_y} + \nu \boldsymbol{\Delta} \boldsymbol{u} \quad (2.1)$$

$$\partial_t \boldsymbol{B} = \boldsymbol{\nabla} \times (\boldsymbol{u} \times \boldsymbol{B}) + \eta \boldsymbol{\Delta} \boldsymbol{B}, \quad (2.2)$$

$$\nabla \cdot \boldsymbol{u} = 0, \quad (2.3)$$

$$\nabla \cdot \boldsymbol{B} = 0. \quad (2.4)$$

This system is written in the incompressible approximation since the MHD turbulence is assumed to be mostly subsonic at the local scale. We also neglect vertical and/or radial stratification for simplicity.

These equations involve the local rotation rate Ω, the local shear rate $S \equiv r\partial r \Omega$, and the local density ρ, assumed to be constant in time and space. Noting that the flow typical length is the height of the simulation box H (this length can crudely be seen as the characteristic height of the global accretion disk), one can define all the dimensionless numbers of the problem :

- The Reynolds number, $Re \equiv SH^2/\nu$, measuring the relative importance of nonlinear coupling through the advection term, and viscous dissipation.
- A proxy to the plasma beta parameter, defined here as $\beta = S^2H^2/V_A^2$ where $V_A^2 = B_o^2/\mu_o\rho$ is the Alfvén speed. The rationale of this definition follows from the vertical hydrostatic equilibrium constraint $c_s \sim \Omega H$, which is expected to hold in thin disks, so that our definition of β is indeed related to the plasma parameter in an equivalent, vertically stratified disk. This parameter measures the relative weight of the Lorentz force and the advection term.
- The rotation number (inverse Rossby number), defined as $R_\Omega = 2\Omega/S$, which measures the relative importance of the Coriolis force.
- The magnetic Reynolds number, $R_m = SH^2/\eta$, which measures the relative importance of resistive dissipation with respect to the ideal term in the induction equation.

We consider only Keplerian disks in this investigation, so that the rotation number is held fixed to its Keplerian value $R_\Omega = -4/3$. This leaves us with three independent dimensionless numbers: β, Re, and Rm. In the following, we will also use the magnetic Prandtl number Pm, which satisfies:

$$Pm \times Re = Rm. \quad (2.5)$$

Lastly, we define the turbulent transport coefficient α as:

$$\alpha = \frac{\langle v_x v_y - B_x B_y/(\mu_o \rho) \rangle}{S^2 H^2}. \quad (2.6)$$

Note that our definition differs slightly from the definition adopted by Hawley et al. (1995) (Eq. 10) due to our S^2H^2 term, leading to a factor $9\gamma/4$ between their definition and Eq. **??**.

2.2 Numerics

The code used for these simulations is an MHD extension of the HD code used in Lesur & Longaretti (2005), and extensively described there. This code is a full 3D spectral (Fourier) code, based on FFTW libraries, parallelized using the MPI protocol. This kind of code has many advantages for the simulation of incompressible turbulence, such as:

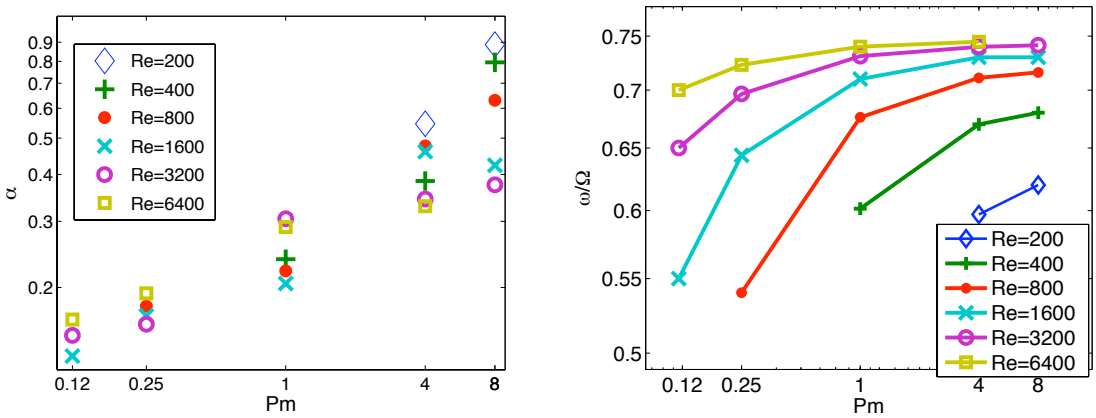

Fig. 1. Transport coefficient (left) and linear growth rate (right) at $\beta = 100$

- The incompressibility and solenoid conditions are easily implemented at machine precision, using a projector function in Fourier space.
- The energy budget is much easier to control, leading to a precise quantification of the energy losses by numerical dissipation.
- Spatial derivatives are very accurate down to the grid scale (equivalent to an infinite order finite difference scheme down to the grid scale).

Comparing our spectral code with a ZEUS-type finite difference code (Stone & Norman 1992), similar results are obtained with a finite difference resolution two to three times larger than the spectral resolution. However, FFT calculations are more computationally expensive than finite differences, leading to a final computational time equivalent for both kind of code with the same "effective" resolution.

All the simulations presented in this paper were performed with an xyz resolution of $128 \times 64 \times 64$ with an aspect ratio of $4 \times 1 \times 1$. One may change the physical viscosity and resistivity as well as the magnetic field intensity (β). The mean magnetic field (conserved in the simulations due to the adopted boundary conditions) is either aligned in the z direction or set equal to zero ($\beta \to \infty$). White noise initial perturbations with respect to the laminar flow are introduced as initial conditions on all variables.

3 Numerical results

3.1 Non zero mean vertical field

All previously published simulations were performed without numerical control of the dissipation scales and dissipation processes. However, such a control is required to ascertain convergence. In this section, the role of the Reynolds and Prandtl numbers is examined. In particular, the Prandtl number allows us to change the ratio of the viscous and resistive dissipation scales. Unfortunately, deviations from $Pm = 1$ are quite demanding numerically, since one wants to resolve both the velocity and magnetic dissipations scales. We present on Fig. **??** (left) the result of such simulations: we plot the mean transport coefficient (α) as a function of the Prandtl number, for various Reynolds numbers (the Reynolds number quantifies the viscous dissipation scale). Statistical averages are computed over 500 shear times, and start after the first 100 shear times to avoid pollution by relaxation of the initial transient dynamics. From these plots, one finds a significant correlation between the Prandtl number and the transport coefficient, leading to

$$\alpha \propto Pm^{\delta} \qquad \text{for} \begin{cases} 0.12 < Pm < 8 \\ 200 < Re < 6400 \end{cases}, \tag{3.1}$$

with δ in the range 0.25 — 0.5. Note that this results shows that the transport coefficient depends on Re and Rm via Pm, at least in the Pm range concidered in this paper. This may be seen on Fig. **??** (left) as a small vertical dispersion (variation of both Re and Rm at constant Pm) compared to the effect of a single Pm change.

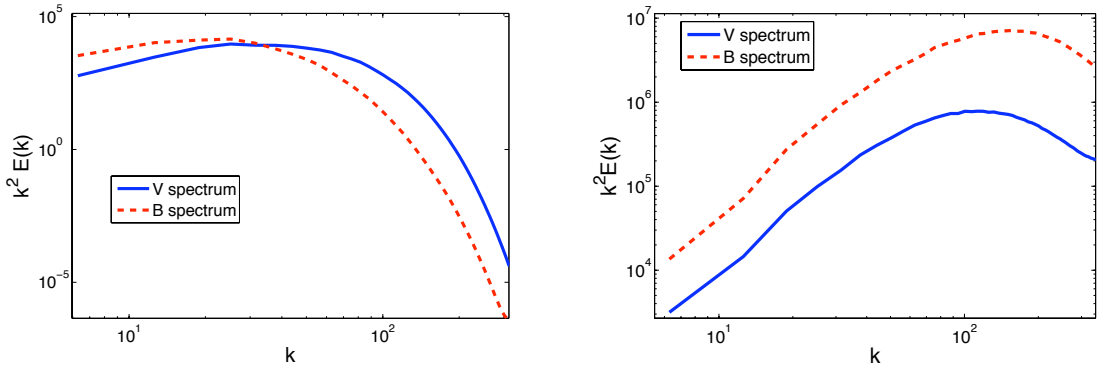

Fig. 2. Dissipation spectrum at $Pm = 0.25$ (left) and $Pm = 4$ (right) for $\beta = 100$

To explain this behaviour, we first try to compare it with the linear growth rate of the most unstable MRI mode (Fig. **??**-right), as linear results are often assumed to control the transport efficiency in astrophysics. Comparing these two plots shows clearly that the $Pm - \alpha$ correlation is not related to the linear behaviour, and is therefore a more complex non-linear phenomenon. To get a closer look at the turbulence dynamics, we plot the dissipation spectrum ($k^2E(k)$) on Fig. **??**. These plots clearly show a maximum at a scale known as the velocity or magnetic field dissipation scale. In particular, we can check that a large Pm correspond to a small magnetic dissipation scale and a large velocity dissipation scale, leading to a possible phenomenology for the $Pm - \alpha$ effect (Lesur & Longaretti 2007).

3.2 Zero mean magnetic field

Despite the fact that one often refers to the MRI in the zero net flux case, the MRI (in the sense of a linear instability) *doesn't exist* without a mean field. The turbulence observed in the zero net flux simulations is due to a non-linear instability involving both a local dynamo effect and a transient MRI growth (see eg. Rincon et al. 2007). However, results from zero-net flux simulation are often considered as the typical MRI turbulence one can expect in a disk (King et al. 2007) since one doesn't need any external field to trigger the instability. In this subsection, we will briefly present some results with zero net flux simulations, using the same code and box as in the previous ones. In particular, we will consider once again a finite viscosity and finite resistivity.

For comparison purposes with the non-zero flux case, we plot on Fig. **??** the temporal evolution of the transport coefficient for three simulation at various Pm, for $Re = 3200$. We first note that both $Pm = 0.25$ and $Pm = 1$ runs lead to a relaminarized flow. More extensive runs, using various kinds of codes and algorithms always lead to flow relaminarization if $Pm < 2$ (Fromang et al. 2007). Note however that these tests always assume a finite (and obviously small, compared to disks) Reynolds numbers. Therefore, these simulations do not necessarily imply that zero magnetic flux MRI turbulence in disks requires $Pm > 2$. However, they show the lack of convergence of previous ideal simulations ($\nu = 0$, $\eta = 0$), for which turbulence was always obtained with this kind of setup, leading to similar results as our $Pm = 4$ run ($\alpha \sim 10^{-3}$).

4 Discussion

In the previous section, we exhibited a correlation between the transport efficiency and the magnetic Prandtl number, leading to a higher transport coefficient for larger Prandtl numbers. In the zero magnetic flux case, simulations with $Pm < 4$ even lead to a relaminarization of the flow, where $\alpha = 0$. However, in spite of our efforts to control numerical artifacts, some approximations may have an important impact on our results. For one thing, the periodic boundary conditions do reinforce the 2D channel flow solution (Goodman & Xu 1994), leading to an artificially large transport efficiency. The incompressibility approximation can have a similar effect, since we neglect sound waves which can act as loss terms for the turbulent field. Lastly, since stratification is neglected, the flow typical length scale is fixed by the cutoff imposed by the box largest length, which is quite different from a classical stratification length. Therefore, one may expect different results when accounting for vertical stratification and possibly when changing the aspect ratio as well.

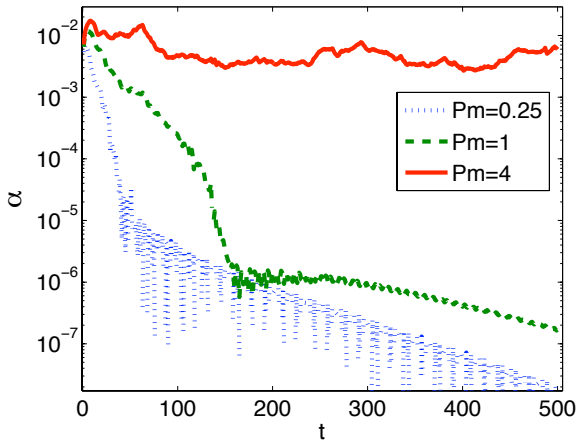

Fig. 3. Temporal evolution of the transport coefficient α for various Prandtl numbers

One should also note that since the shearing-box approximation imposes a constant mean magnetic field in the simulation, dynamo effects can't show up on this field. Therefore, the magnetic field topology in local simulations is an external constraint; one may possibly expect a real disk to switch locally from non-zero and zero mean field configurations (or vice-versa). This remark leads us to conclude that the efficiency of the MRI-induced turbulence in real disks may be highly variable, as one can get $\alpha \sim 5 \times 10^{-3}$ in $Pm > 2$ zero flux configurations up to $\alpha \sim 0.6$ for $Pm = 4$ non zero flux (at least, as these variations are limited by the parameter space available in our simulations). Moreover, these values have a large error bar due to the numerical artifacts discussed above, and also due to the very low Reynolds numbers that can be reached in our simulations ($Re \sim 10^3$ in simulation whereas $Re > 10^{10}$ in disks). Therefore, even the most resolved simulations achievable on present day computers cannot ascertain whether MRI is able to explain the observed transport in magnetised disks $\alpha \sim 10^{-2}$—1 (King et al 2006).

The simulations presented in this paper have been performed both at IDRIS (French national computational center) and at the SCCI (Grenoble Observatory computational center). The authors acknowledge fruitful discussions on the issues discussed here with Steve Balbus, Sébastien Fromang and John Papaloizou.

References

Balbus, S.A., & Hawley, J.F. 1991, ApJ, 376, 214
Balbus, S.A., Hawley, J.F., & Stone, J.M. 1996, ApJ, 467, 76
Fromang, S., Papaloizou, J., Lesur, G., & Heinemann, T. 2007, MNRAS, submitted (ArXiv 0705.3622)
Goldreich, P. & Lynden-Bell, D. 1965, MNRAS, 130, 125
Goodman, J., & Xu, G. 1994, ApJ, 432, 213
Hawley, J.F. 2000, ApJ, 528, 462
Hawley, J.F., Balbus, S.A., & Winters, W.F. 1999, ApJ, 518, 394
Hawley, J.F., Gammie, C. F., & Balbus, S.A. 1995, ApJ, 440, 742
King, A.R, Pringle, J.E., & Livio, M. 2007, MNRAS, 376, 1740
Lesur, G., & Longaretti, P-Y. 2005, A&A, 444, 25
Lesur, G., & Longaretti, P-Y. 2007, MNRAS, 378, 1471
Richard, D., & Zahn, J-P. 1999, A&A, 347, 734
Rincon, F., Ogilvie, G.I., & Cossu, C. 2007, A&A, 463, 817
Shakura, N.I., & Sunyaev, S.A. 1973, A&A, 24, 337
Stone, J.M., Hawley, J.F., Gammie, C.F., & Balbus, S.A. 1996, ApJ, 463, 656
Stone, J.M. & Norman, M.L. 1992, ApJs, 80,753